ACS OMEGA

http://pubs.acs.org/journal/acsodf

Article

Chemical and Morphological Modifications Induced by Argon Plasma Treatments on Fluorinated Polybenzoxazole Films

Francesco Perricelli, Massimo Boscaglia, Massimiliano Cantiano, Luca Spitaleri, Maria Elena Fragalà, and Antonino Gulino*

Cite This: *ACS Omega* 2023, 8, 15586−15593

Read Online

ACCESS | Metrics & More | Article Recommendations | Supporting Information

ABSTRACT: Fluorinated photodefinable polymers are widely employed as re-distribution layers in wafer-level packaging to produce microelectronic devices because of their suitable low dielectric constant and moisture absorption, high mechanical toughness, thermal conductivity and stability, and chemical inertness. Typically, fluorinated photodefinable polybenzoxazoles (F-PBOs) are the most used in this field. In the present work, we investigated by atomic force microscopy, X-ray photoelectron spectroscopy, and Fourier transform infrared spectroscopy the morphological and chemical modifications induced by Ar plasma treatments on F-PBO films. This process, used to remove surface contaminant species, as well as increase the polymeric surface roughness, to improve the adhesion to the other components during electronic packaging, is a crucial step during the manufacturing of some microelectronic devices. We found that argon plasma treatments determine the wanted drastic increase of the polymer surface roughness but, in the presence of a patterned silver layer on F-PBO, needed for the fabrication of electric contacts in microelectronic devices, also induce some unwanted formation of silver fluoride species.

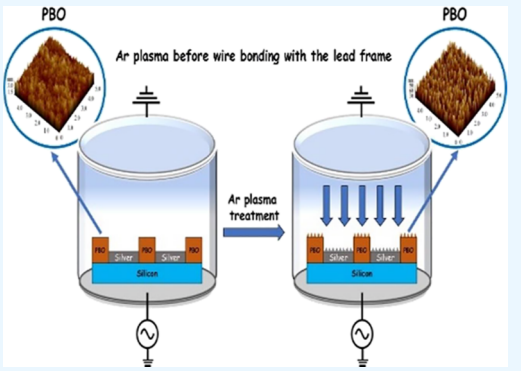

INTRODUCTION

In recent years, the fabrication of integrated circuits (ICs) has increased in response to the growing demand for micro-electronic devices, such as smartphones, tablets, laptops, flexible electronics, and electric vehicles.[1,2] The newest generation of microelectronic devices is characterized by the increase in device density and fabrication complexity but, simultaneously, by the decrease in thickness and dimensions.[3] This condition represents a challenge for the fan-out wafer-level package, which requires the employment of electronic packaging materials with low dielectric properties, also able to dissipate heat.[4]

Microelectronic packaging represents an important step during the fabrication of microelectronic devices because it provides the electrical connection/isolation, mechanical support, thermal cooling, and physical protection of the electronic components. Therefore, the performance of a power module depends also on the electrical, thermal, and mechanical properties of the packaging materials.[5,6]

Dielectric polymers have widely been employed in the fabrication of microelectronic devices, such as buffer coatings, passivation layers, alpha particle barriers, and re-distribution layers in wafer-level packaging. In fact, they show suitable features such as low dielectric constant, high mechanical toughness, high thermal conductivity and stability, low moisture absorption, good adhesion to substrates, and chemical inertness. Moreover, their low thermal expansion coefficient is also important to minimize the stress arising because of the thermo-mechanical mismatch between the device and the packaging constituents.[7,8]

Photodefinable dielectric polymers represent the most important class of materials used in microelectronic packaging and can be produced by the functionalization of the oligomer backbone with photosensitive moieties.[9,10]

Furthermore, the presence of fluorine groups in the polymer induces, at the same time, the reduction of polymeric dielectric permittivity.[11−14] In this context, photodefinable polybenzoxazoles (PBOs) are a particular class of stable-at-high-temperature, dielectric polymers formed by phenylene groups and condensed aromatic heterocyclic rings.[15−18]

The final step of the device fabrication is represented by the packaging process. Before this packaging, the removal of eventual contaminants present on the device surface is important.[19] Worldwide leaders for semiconductors and electronic integrated device manufacturers currently employ

Received: February 13, 2023
Accepted: March 28, 2023
Published: April 21, 2023

plasma cleaning treatments to remove all kinds of surface contaminant species. After the plasma cleaning and before the packaging, the most widespread interconnected technology, used to assemble an IC, is the wire-bonding process that consists of soldering metallic wires between the single device and the lead frame that constitutes the skeleton of the package.[20] In addition to the removal of the surface contaminants, plasma cleaning treatments are also employed to roughen the polymeric surface on the nanometric scale in order to improve the adhesion by mechanical interlocking between PBO and the other components of the electronic packaging.[21] However, the plasma treatment can determine some disadvantages, which include the potential damage of the PBO chemical structure and the production of collateral species that contaminate the device surface.

In the above context, the aim of this work was to investigate the surface chemical modifications induced by the Ar plasma treatments on a model system consisting of an F-PBO layer with a patterned silver layer on it (Scheme 1). The F-PBO polymer is widely employed in the manufacturing of microelectronic devices, and that used in this work belongs to the patented HD-8820 series, developed by HD Micro-Systems, and used for semiconductor stress buffer and packaging applications. The characterization was performed by Fourier transform infrared spectroscopy (FT-IR), X-ray photoelectron spectroscopy (XPS), and atomic force microscopy (AFM).

Scheme 1. Synthetic Pathway for the Patterned F-PBO-Silver System[a]

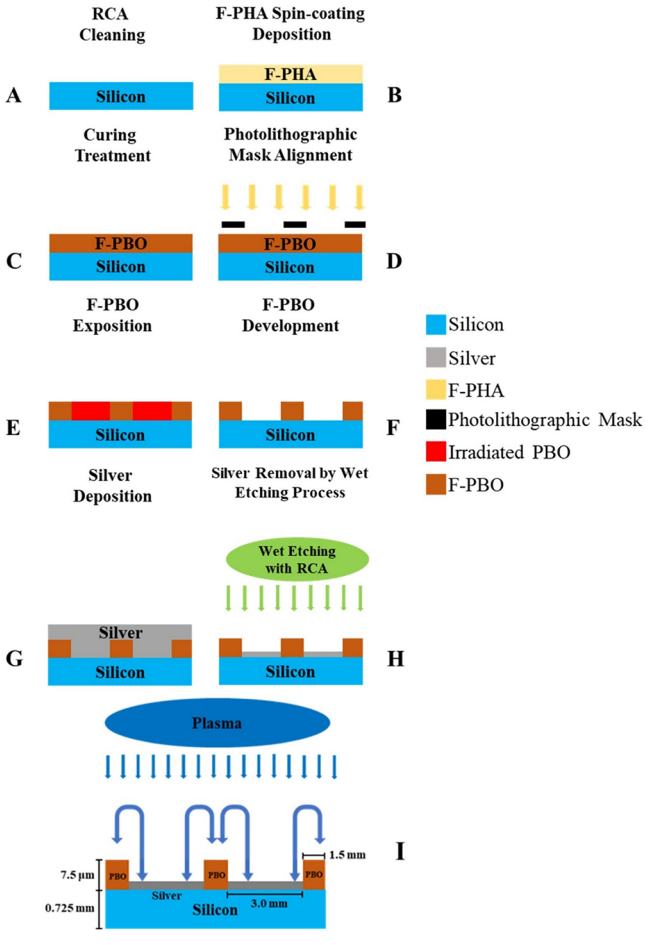

[a](A) RCA cleaning; (B) F-PHA spin-coating deposition; (C) curing treatment; (D) photolithographic mask alignment; (E) F-PBO exposition; (F) F-PBO development; (G) silver deposition; (H) silver removal by the wet etching process; (I) Ar plasma treatment; see also Scheme S1.

EXPERIMENTAL METHODS

Fabrication of the Patterned F-PBO-Silver Model System. Scheme 1 illustrates the manufacturing steps adopted to produce a patterned fluorinated F-PBO-silver model system on a commercial 8" Si substrate, and the following procedure is that adopted by STMicroelectronics, which is one of Europe's largest electronic and semiconductor manufacturers. Note that the exact formulation of the fluorinated PBO used in this work is patented and its composition is, therefore, company-restricted. However, from the datasheet of the HD-8820 polymer, it is possible to identify the main components of this polymeric blend. To sum up, the polymeric blend is composed of a fluorinated (o-hydroxyamide) (F-PHA), which represents the polymer precursor, and a diazonaphthoquinone-based photoacid generator (DNQ-PAG), both solubilized in a solvent mixture of propylene glycol methyl ether acetate and gamma-butyrolactone.[9,15,17]

The synthetic pathway for the patterned F-PBO-silver system is as follows: first, the Si substrate was subjected to a standard cleaning with an RCA solution (H_2O/H_2O_2 30%/NH_3 28%, 5:1:1 v/v/v)[22−24] to remove eventual contaminants on the wafer surface (Scheme 1A). Next, a uniform and homogeneous F-PHA prepolymer film was deposited on the surface of the Si wafer using a Silicon Valley Group spin coater (Scheme 1B). The spin-coating conditions were as follows: spinning rate = 1200 revolutions per minute (rpm); temperature = 25 °C; spin-coating time = 30 s; and F-PHA concentration in the polymer solution = 35% w/w. Next, the polymeric film was soft-baked on a hot plate at 120 °C for 3 min and thermally cured at 320 °C 1 h in a nitrogen (N_2) atmosphere to produce the F-PBO cured film (Scheme 1C). After the curing process, specific portions of the F-PBO layer were protected with a quartz mask (Scheme 1D), and a lithography step was performed to pattern the polymeric film (Scheme 1E). Specifically, the F-PBO film was irradiated with UV light (wavelength = 365 nm and power exposition = 800 mJ/cm^2, 120 s). Upon UV light exposure, the DNQ-PAG undergoes a rearrangement reaction, which causes the increase of the polymer solubility in the exposed portions.[9,15,17,18] After that, the exposed polymeric zones were developed with a 3.5% aqueous solution of tetramethylammonium hydroxide ($(CH_3)_4N(OH)$) (Scheme 1F).[15,17] At this point, a silver (Ag) layer was deposited on the F-PBO patterned film using a physical sputtering deposition process by means of the TEL (Tokyo Electron Limited)-metal sputter system (Scheme 1G). The deposition parameters were as follows: chamber pressure = 1.33 × 10^{-5} Pa and bias power = 5000 W. Then, a wet etching process, performed with an RCA standard solution, was carried out to totally remove the Ag layer on the top of the F-PBO layer and reduce the thickness to 1.5 μm of the Ag layer present on the Si surface (Scheme 1H). Finally, on the patterned F-PBO-silver model system surface, an Ar plasma treatment (Scheme 1I) in a LAM-poly etcher was performed, as schematized in Figure 1. Plasma parameters were as follows: chamber pressure = 2.67 Pa, bias power range = 80−150 W, Ar flux = 100 sccm, and exposition time = 100 s.

https://doi.org/10.1021/acsomega.3c00952
ACS Omega 2023, 8, 15586−15593

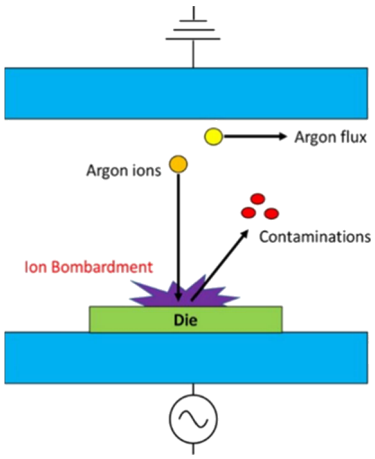

Figure 1. Graphical schematization of the Ar plasma cleaning treatment.

X-ray Photoelectron Spectroscopy. X-ray photoelectron (XP) spectra were measured at a 45° take-off angle relative to the surface sample holder, with a PHI 5600 Multi Technique System (Physical Electronics GmbH, Feldkirchen, Germany; the base pressure of the main chamber was 3×10^{-8} Pa).[25−27] Samples, placed on a molybdenum specimen holder, were excited with Al Kα X-ray radiation using a pass energy of 5.85 eV. The instrumental energy resolution was ≤0.5 eV. Structures due to the Al Kα X-ray satellites were subtracted prior to data processing. XPS peak intensities were obtained after Shirley background removal.[25,26] Spectral calibration was achieved by fixing the Ag $3d_{5/2}$ peak of a clean sample at 368.3 eV; this method turned the C 1s peak of the adventitious carbon contamination at 285.0 eV.[25−27] No charging effect during the XPS analyses was observed since the PBO film is on silicon, and the molybdenum sample holder is conducting. In addition, the F-PBO film is patterned with silver for the electric contacts with the lead frame. The atomic concentration analysis was performed by considering the relevant atomic sensitivity factors. The fitting of some XP spectra was carried out, using the XPSPEAK4.1 software, by fitting the spectral profiles with symmetrical Gaussian envelopes, after subtraction of the background. This process involves data refinement, based on the method of the least-squares fitting, carried out until there was the highest possible correlation between the experimental spectrum and the theoretical profile. The residual or agreement factor R, defined by $R = [\Sigma (F_{obs} - F_{calc})^2/\Sigma (F_{obs})^2]^{1/2}$, after minimization of the function $\Sigma (F_{obs} - F_{calc})^2$ converged to the value of 0.03.

Atomic Force Microscopy. The morphology of the F-PBO film was observed by AFM using a Solver P47 NT-MDT instrument. The noise level before and after each measurement was 0.01 nm. AFM characterization was performed in a high-amplitude mode (tapping mode and resonance frequency of 150.0 Hz).

Fourier Transform Infrared Spectroscopy. FT-IR spectra were recorded using a 4600 Jasco FT/IR-430 spectrometer in the 4000−400 cm^{-1} scan range, with an instrumental resolution of 4 cm^{-1}.

RESULTS AND DISCUSSION

The cyclization of the chemical structure of the F-PHA polymer precursor, responsible for the formation of the cured F-PBO film, was evaluated by XPS and FT-IR analyses. The XPS technique is ideal for an accurate description of the surface electronic structure and to identify the chemical composition once the relevant atomic sensitivity factors have been considered.[22−29] Figure 2 shows the high-resolution XP spectra of the F-PHA polymer precursor and cured F-PBO films in the C 1s binding energy region.[30] A careful fitting of the experimental profile of the C 1s signal of the F-PHA polymer precursor film required five Gaussian components centered at 285.0, 286.6, 288.6, 290.8, and 292.8 eV, respectively (Figure 2A). The first component at 285.0 eV is due to the C−C/C−H bonds of the F-PHA backbone.[25,26] The peaks at 286.6 and 288.6 eV are assigned to the C−OH and amide (O=C−N−H) groups, respectively.[31,32] The other peaks at 290.8 and 292.8 eV are due to the $-CF_2$ and $-CF_3$ groups.[33] Figure 2B shows the XP spectrum of the F-PBO cured film in the C 1s binding energy region. There is evidence of four Gaussian components at 285.0, 287.0, 290.8, and 292.8 eV, respectively. The first component (285.0 eV) is due to the C−C/C−H bonds of the F-PBO backbone. The second peak at 287.0 eV is assigned to the carbon of the benzoxazole ring (−N=C−O−).[34] The presence of this signal, consequently with the disappearance of the signals due to the C−OH and amide (O=C−N−H) groups (286.6 and 288.6 eV), confirms the cyclization of the polymeric backbone with the formation

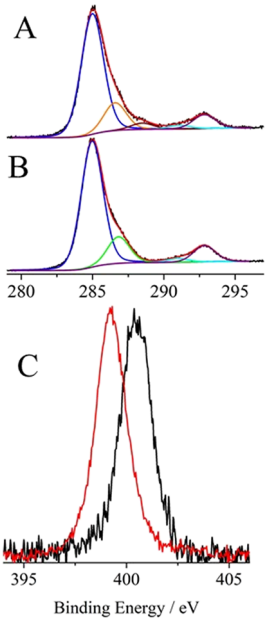

Figure 2. (A) Al Kα excited XPS of the F-PHA polymer precursor film in the C 1s energy region. The black line refers to the experimental profile; the Gaussians at 285.0 eV (blue line), 286.6 eV (orange line), 288.6 eV (wine line), 290.8 eV (cyan line), and 292.8 eV (purple line) represent the five C 1s components; the red line, superimposed to the experimental profile, refers to the sum of the Gaussian components. (B) Al Kα excited XPS of the cured F-PBO film in the C 1s binding energy region. The black line refers to the experimental profile; the Gaussians at 285.0 eV (blue line), 287.0 eV (green line), 290.8 eV (cyan line), and 292.8 eV (purple line) represent the four C 1s components; the red line, superimposed to the experimental profile, refers to the sum of the Gaussian components. (C) Al Kα excited XPS of the F-PHA polymer precursor film (black line) and the cured F-PBO film (red line) in the N 1s energy region. The two spectra have been normalized to the same intensity.

https://doi.org/10.1021/acsomega.3c00952
ACS Omega 2023, 8, 15586−15593

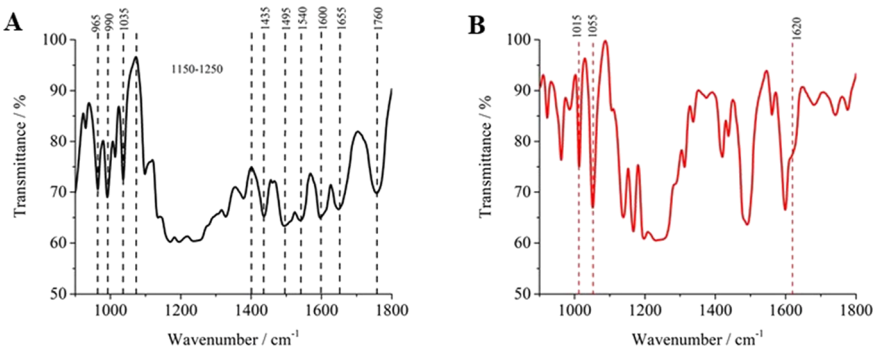

Figure 3. FT-IR spectra of the F-PHA precursor film (A), before the thermal curing process, and (B) of the F-PBO film, after the thermal curing process, measured in the 900−1800 cm^{-1} range.

of the benzoxazole ring (Scheme S1). Finally, the peaks at 290.8 and 292.8 eV are in analogy with those observed for the F-PHA polymer precursor. Figure 2C shows the high-resolution XP spectra of the F-PHA polymer precursor and cured F-PBO films in the N 1s binding energy. The N 1s spectrum of the F-PHA polymer precursor shows one clear band centered at 400.5 eV due to the amide group O═C−N−H,[31,32] while the N 1s signal of the F-PBO film after curing at 320 °C shows a clear band at 399.3 eV due to the benzoxazole ring (−N═C−O−).[35] This experimental observation confirms the cyclization of the polymeric backbone and, hence, the success of the thermal curing treatment.

Both high-resolution XP spectra of the F-PHA polymer precursor and cured F-PBO films in the F 1s binding energy region (Figure S1) showed a band centered at 688.9 eV due to the C−F bonds present in the polymeric structure.[33]

Figure S2 shows the high-resolution XP spectra of the F-PHA polymer precursor and cured F-PBO films in the oxygen 1s region. The O 1s spectral profile of the F-PHA precursor was fitted using two Gaussian components centered at 531.9 and 533.5 eV, respectively. The first component at 531.9 eV corresponds to the oxygen of the amide group (O═C−N−H),[31,32] while the higher energy peak, located at 533.5 eV, is assigned to C−OH species.[31,36] The O 1s spectrum of the cured F-PBO film at 320 °C shows one clear band centered at 532.7 eV due to the oxygen of the benzoxazolic ring (Figure S2B).[35]

The chemical modifications occurring in the F-PHA films during the thermal curing process were also monitored using FT-IR analysis.[37,38] Figure 3A shows the FT-IR spectrum of the F-PHA polymer precursor film before the thermal curing process, measured in the 900−1800 cm^{-1} range. In particular, this FT-IR spectrum shows the characteristic absorption peaks of the fluorinated poly-hydroxy-amide precursor at 965 cm^{-1} (C−H bending), 990 cm^{-1} (C═C bending), 1035 cm^{-1} (C−O−H stretching), 1150−1250 cm^{-1} (C−F stretching), 1435 cm^{-1} (C−O−H bending), 1495 cm^{-1} (C−F bending), 1540 cm^{-1} (amide I stretching), 1600 cm^{-1} (aromatic C═C stretching), 1650 cm^{-1} (amide II stretching), and 1760 cm^{-1} (C═O stretching).[39−41]

Figure 3B shows the FT-IR spectrum of the F-PBO film after the thermal curing process and suggests that several distinct changes occur during the thermal curing process. More specifically, the absorption peaks characteristic of the amide functionality disappear, while, simultaneously, the typical signals of the benzoxazole ring structure appear at 1015 cm^{-1} (−C−O−C− stretching), 1055 cm^{-1} (benzoxazole ring −C−O−C− stretching), and 1620 cm^{-1} (benzoxazole ring −C═N− stretching).[39−41] The latter peak interferes with the aromatic C═C stretching peak centered at 1600 cm^{-1}.

The surface morphology of the F-PHA polymer precursor and cured F-PBO films was also investigated by AFM, as shown in Figure 4. The F-PHA polymer precursor film is

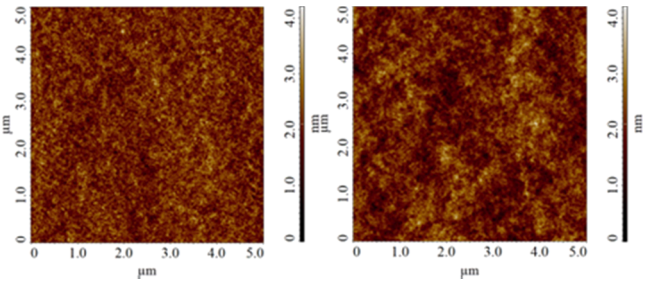

Figure 4. AFM images of the F-PHA precursor film (left) and the F-PBO film after thermal curing treatment (right).

characterized by a root mean square (RMS) value of 0.26 nm and a peak-to-peak (PtP) value of 2.14 nm, while the cured F-PBO film shows an RMS value of 0.48 nm with a PtP value of 4.20 nm. Considering these data, it is possible to affirm that the thermal curing process has also produced a slight increase in the surface roughness.

As reported before, a relevant increase in the surface roughness of the dielectric polymer and the simultaneous removal of eventual contaminants present on the surface of the microelectronic devices are generally performed by Ar plasma treatments. Therefore, we studied by AFM the variation of the surface morphology of the F-PBO film also after the plasma treatment, and Table 1 summarizes the RMS values of the F-PBO film, upon varying the bias power, after this process.

Table 1. Comparison of the RMS and PtP Values of the F-PBO-Silver Model System, upon Different Ar Plasma Bias Powers

experiment	bias power [W]	exposition time [s]	root mean square [nm]	peak-to-peak [nm]
0	0	0	0.48	4.20
1	80	100	9.69	68.52
2	100	100	12.52	85.81
3	120	100	13.83	94.90
4	150	100	14.64	100.46

https://doi.org/10.1021/acsomega.3c00952
ACS Omega 2023, 8, 15586−15593

It emerges that the surface roughness of the F-PBO film tends to increase with the growth of the bias power. Figure S3 shows the AFM image of the F-PBO-silver model system on the polymer zone after the Ar plasma experiment 4 in which the experimental conditions are argon flux = 100 sccm, bias power = 150 W, and argon plasma treatment time = 100 s. The polymeric surface is characterized by the highest RMS and PtP values of 14.64 and 100.46 nm, respectively.

At the same time, we carried out the morphological analysis of the F-PBO-silver model on the metal zone surface by using AFM. Figure S4 shows the AFM images of the F-PBO-silver model system on the metal zone before and after the Ar plasma treatment. Before the Ar plasma treatment, the metal surface is characterized by an RMS value of 6.32 nm and a PtP value of 50.43 nm, while after the plasma treatment, the metal surface shows an RMS value of 12.41 nm and a PtP value of 169.69 nm. Therefore, it clearly appears that the Ar plasma treatment also determines a significant increase in the silver surface roughness.

Considering the previous data, we repeated the surface chemical analysis by XPS on the F-PBO-silver model system after the Ar plasma treatment (experiment 4). Figure 5 shows

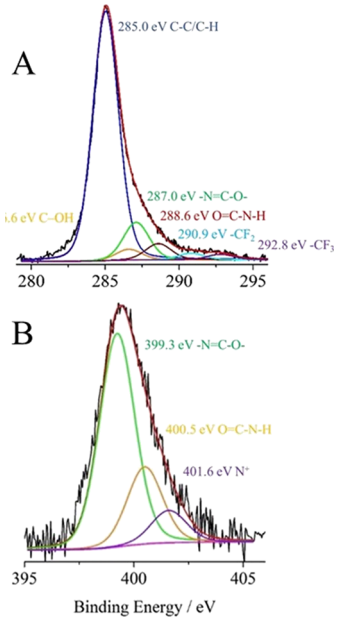

Figure 5. (A) Al Kα excited XPS of the F-PBO-silver model system after the Ar plasma treatment on the polymer zone in the C 1s energy region. The black line refers to the experimental profile; the Gaussians at 285.0 eV (blue line), 286.6 eV (orange line), 287.0 eV (green line), 288.6 eV (wine line), 290.9 eV (cyan line), and 292.8 eV (purple line) represent the five C 1s components. (B) Al Kα excited XPS of the F-PBO-silver model system after the Ar plasma treatment on the polymer zone in the N 1s energy region. The green, orange, and violet lines refer to the 399.3, 400.5, and 401.6 eV components; the magenta line refers to the background; in both cases, the red line superimposed on the experimental black profile refers to the sum of all Gaussian components.

the high-resolution XP spectrum of the F-PBO-silver model system on the polymer zone in the C 1s binding energy region. The spectrum revealed five Gaussian components centered at 285.0, 286.6, 287.0, 288.6, 290.8, and 292.8 eV, respectively. The presence of the C−OH (286.6 eV) and amide (O=C−N−H) (288.6 eV) groups is due to some partial breakage of the benzoxazole ring that partially restored some F-PHA. The intensities of the components at 290.8 and 292.8 eV ($-CF_2$ and $-CF_3$ groups) drastically decreased to one-tenth of those before the plasma due to the surface depletion of the fluorine atoms induced by the Ar plasma treatment.

Figure 5B shows the high-resolution XP spectrum of the F-PBO-silver model system on the polymer zone after Ar plasma treatment in the N 1s binding energy region. The N 1s spectral profile was fitted using three Gaussian components at 399.3, 400.5, and 401.6 eV, respectively. The reappearing of the peak of the amide group (O=C−N−H) at 400.5 eV confirms the partial breakage of the benzoxazolic ring. The higher-energy, low-intensity peak, located at 401.6 eV, in tune with a large crop of literature data, is due to the quaternized nitrogen (N^+).[41−44]

Figure 6A shows the high-resolution XPS of the F-PBO-silver model system on the polymer zone after Ar plasma

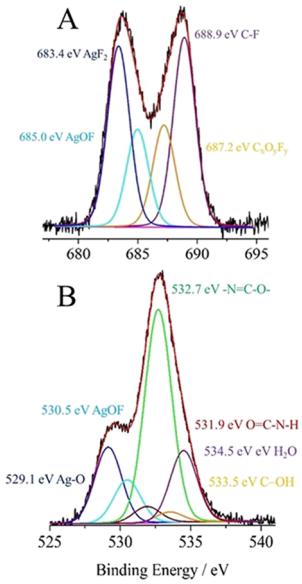

Figure 6. (A) Al Kα excited XPS of the F-PBO-silver model system after the Ar plasma treatment on the polymer zone in the F 1s energy region. The blue, cyan, orange, and purple lines refer to 683.4, 685.0, 687.2, and 688.9 eV components; the magenta line refers to the background. (B) Al Kα excited XPS of the F-PBO-silver model system after the Ar plasma treatment on the polymer zone in the O 1s binding energy region. The blue, cyan, wine, green, orange, and purple lines refer to 529.1, 530.5, 531.9, 532.7, 533.5, and 534.5 eV components. In both cases, the red line superimposed on the experimental black profile refers to the sum of all Gaussian components.

treatment in the F 1s binding energy region. Four Gaussian components centered at 683.4, 685.0, 687.2, and 688.9 eV are evident. The first component at 683.4 eV is due to the formation of silver fluorides AgF_2,[45] while the second component at 685.0 is assigned to silver oxyfluoride AgOF species (vide infra).[46] These species were produced by the reaction of the fluorine atoms present in the F-PBO film and the silver layer. The third component at 687.2 eV is ascribed to fluoro-hydrocarbon $C_xO_yF_y$ species having different stoichiometry.[33] Finally, the last component at 688.9 eV is due to the C−F groups present in the polymeric structure.

Figure 6B shows the high-resolution XPS of the F-PBO-silver model system on the polymer zone in the O 1s energy

https://doi.org/10.1021/acsomega.3c00952
ACS Omega 2023, 8, 15586−15593

region. A precise fitting of this spectrum required six Gaussian components centered at 529.1, 530.5, 531.9, 532.7, 533.5, and 534.5 eV, respectively. The first component (529.1 eV) is due to the oxygen of silver oxide Ag−O species, while the second component at 530.5 is ascribed to the oxygen of the silver oxyfluoride AgOF species.[46,47] The peak at 531.9 eV is due to the oxygen of the amide group (O═C−N−H), the peak centered at 532.7 eV is assigned to the benzoxazolic ring (−N═C−O−), and the peak at 533.5 is ascribed to the C−OH species. According to the previous XPS measurements, the presence of the C−OH and amide (O═C−N−H) groups is due to some partial breakage of the benzoxazole ring. Finally, the last peak at 534.5 eV reveals the presence of water molecules on the polymer surface.[26,39]

Figure S5 shows the high-resolution XP spectrum of the F-PBO-silver model system on the metal zone before the Ar plasma treatment. This spectrum shows the Ag $3d_{5/2,3/2}$ spin−orbit components at 368.6 and 374.6 eV (6.0 eV spin−orbit coupling), in tune with the presence of Ag^0 states.[46−48] After the Ar plasma treatment, no significant modifications appear on the XP spectrum in the Ag 3d energy region, as shown in Figure S6.

Before the plasma treatment, as expected, there was no XPS signal of any silver species on the PBO zone. After the Ar plasma treatment, also on the polymer zone (Figure 7), there

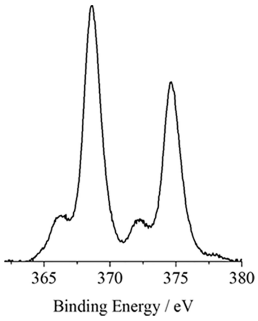

Figure 7. Al Kα excited XPS of the F-PBO-silver model system after Ar plasma treatment on the polymer zone in the Ag 3d energy region.

was evidence of a small presence (~2%) of the Ag $3d_{5/2,3/2}$ spin−orbit components at 368.6 and 374.6 eV (6.0 eV spin−orbit coupling). In addition, the presence of other Ag $3d_{5/2,3/2}$ spin−orbit shoulders centered at 366.2 and 372.2 eV (6.0 eV spin−orbit coupling) indicates some Ag^{2+} states (silver fluorides AgF_2 and silver oxyfluorides AgOF).[45−48] Binding energy shifts opposite (negative) to those expected on the basis of formal charges, upon increasing the silver oxidation state for the Ag 3d peaks, were already observed in XPS data.[45−47]

Therefore, one of the key findings in this manuscript is a small but sizeable reaction of silver and F-PBO as a result of plasma treatment. In fact, when the polymer film is deposited by spin coating, the centrifugal force produces a partial segregation of the fluorinated moieties on the film surface because the entropic cost of the fluorinated groups migrating to the polymer/air interface is reduced during the film formation.[49] Then, the Ar plasma process was used both to clean the surface and to improve the interfacial adhesion of the polymer.[50] This process removes some silver atoms from the metallic layer and mixes them with/on the polymer surface, thus promoting the formation of silver fluorides.

Considering the previous data, the Ar plasma treatment of the F-PBO-silver model system induces drastic modification of the morphological and chemical features of the F-PBO surface. More specifically, we noted a partial breakage of the benzoxazolic rings and some depletion of fluorine species from the surface. On the other hand, some oxidized silver particles are now present on the polymer surface. It is fundamental to recall that the RMS before the plasma treatment was 0.48 nm, while after the plasma, it reached a value of 14.64 nm and this surface roughness increase was one of the main purposes of the present plasma treatment.

CONCLUSIONS

The main aim of this work was to study the modification of the morphological and chemical surface structure of the F-PBO film deposited on the surface of microelectronic devices after thermal curing and Ar plasma treatment. The last process is used to increase the polymeric surface roughness and improve the adhesion to the other components during the electronic packaging. After thermal curing at 320 °C, we mainly noted the disappearance of the signal of the amide group (O═C−N−H) and the appearance of the signal of the benzoxazole ring (−N═C−O−). Furthermore, a drastic increase of the surface roughness of the F-PBO film and, at the same time, the formation of some silver fluorides on its surface have been observed. The observed presence of some silver species on the polymer zone was found to be negligible.

ASSOCIATED CONTENT

Supporting Information

The Supporting Information is available free of charge at https://pubs.acs.org/doi/10.1021/acsomega.3c00952.

Main changes in the chemical species; XPS of F-PHA and cured F-PBO films in the F 1s energy region and the O 1s energy region; AFM images of the F-PBO-silver model system on the polymer zone after the Ar plasma treatment and the metal zone before and after the Ar plasma treatment; and XPS of the F-PBO-silver model system before and after the Ar plasma treatment on the metal zone in the Ag 3d energy region (PDF)

AUTHOR INFORMATION

Corresponding Author

Antonino Gulino − *Department of Chemical Sciences, University of Catania, 95125 Catania, Italy; INSTM UdR of Catania, 95125 Catania, Italy;* orcid.org/0000-0002-6850-3080; Phone: +39-095-7385067; Email: agulino@unict.it; Fax: +39-095-580138

Authors

Francesco Perricelli − *STMicroelectronics Stradale Primosole, 95121 Catania, Italy*

Massimo Boscaglia − *STMicroelectronics Stradale Primosole, 95121 Catania, Italy*

Massimiliano Cantiano − *STMicroelectronics Stradale Primosole, 95121 Catania, Italy*

Luca Spitaleri − *STMicroelectronics Stradale Primosole, 95121 Catania, Italy*

Maria Elena Fragalà − *Department of Chemical Sciences, University of Catania, 95125 Catania, Italy; INSTM UdR of Catania, 95125 Catania, Italy;* orcid.org/0000-0001-9414-7780

https://doi.org/10.1021/acsomega.3c00952
ACS Omega 2023, 8, 15586−15593

Complete contact information is available at:
https://pubs.acs.org/10.1021/acsomega.3c00952

Author Contributions

The manuscript was written through contributions of all authors. All authors have given approval to the final version of the manuscript.

Funding

University of Catania, PIA.CE.RI. project 2020−2022, European Union (NextGeneration EU), MUR-PNRR project SAMOTHRACE (ECS00000022), and the B.R.I.T. for the XPS facility.

Notes

The authors declare no competing financial interest.

■ ACKNOWLEDGMENTS

The authors thank the University of Catania for the financial support of the PIA.CE.RI. MAF-MOF project 2020−2022 and the B.R.I.T. laboratory of the University of Catania for the availability of the XPS facility. This work has also been partially funded by European Union (NextGeneration EU) through the MUR-PNRR project SAMOTHRACE (ECS00000022).

■ REFERENCES

(1) Keser, B.; Kröhnert, S. Embedded and Fan-Out. *Wafer and Panel Level Packaging Technologies for Advanced Application Spaces: High Performance Compute and System in Package*; The Institute of Electrical and Electronics Engineers, Inc., 2022.

(2) Jeong, G.; Park, J.; Lee, S.; Kim, P.; Han, M.; Hong, S.; Kim, E.; Park, J.; Choo, B.; Kang, S.; Park, J.-G. Polymer link breakage of polyimide film surface using hydrolysis reaction accelerator for enhancing chemical−mechanical-planarization polishing rate. *Sci. Rep.* **2022**, *12*, 3366.

(3) Pirnaci, M. D.; Spitaleri, L.; Tenaglia, D.; Perricelli, F.; Fragalà, M. E.; Bongiorno, C.; Gulino, A. Systematic Characterization of Plasma-Etched Trenches on 4H-SiC Wafers. *ACS Omega* **2021**, *6*, 20667−20675.

(4) Li, R.; Yang, X.; Shen, Y.; Zhang, L.; Wang, C.; Zheng, X.; Chen, H.; Zhang, T. Review on polymer composites with high thermal conductivity and low dielectric properties for electronic packaging. *Mater. Today Phys.* **2022**, *22*, No. 100594.

(5) Qu, S.; Liu, Y. *Wafer-Level Chip-Scale Packaging: Analog and Power Semiconductor Applications*; Springer: New York, 2015.

(6) Calabretta, M.; Sitta, A.; Oliveri, S. M.; Sequenzia, G. Silver Sintering for Silicon Carbide Die Attach: Process Optimization and Structural Modeling. *Appl. Sci.* **2021**, *11*, 7012.

(7) Wang, T.; Li, J.; Niu, F.; Zhong, A.; Liu, J.; Liu, W.; Shan, L.; Zhang, G.; Sun, R.; Wong, C. Low-temperature curable and low-dielectric polyimide nanocomposites using aminoquinoline-functionalized graphene oxide Nanosheets. *Compos. B. Eng.* **2022**, *228*, No. 109412.

(8) Bei, R.; Qian, C.; Zhang, Y.; Chi, Z.; Liu, S.; Chen, X.; Xu, J.; Aldred, M. P. Intrinsic low dielectric constant polyimides: relationship between molecular structure and dielectric properties. *J. Mater. Chem. C* **2017**, *5*, 12807.

(9) Fu, M.-C.; Higashihara, T.; Ueda, M. Recent progress in thermally stable and photosensitive polymers. *Polym. J.* **2018**, *50*, 57−76.

(10) Zhang, K.; Han, L.; Froimowicz, P.; Ishida, H. A Smart Latent Catalyst Containing o-Trifluoroacetamide Functional Benzoxazine: Precursor for Low Temperature Formation of Very High Performance Polybenzoxazole with Low Dielectric Constant and High Thermal Stability. *Macromolecules* **2017**, *50*, 6552−6560.

(11) Zhang, F.; Li, J.; Wang, T.; Huang, C.; Ji, F.; Shan, L.; Zhang, G.; Sun, R.; Wong, C. Fluorinated graphene/polyimide nanocomposites for advanced electronic packaging applications. *J. Appl. Polym. Sci.* **2021**, *138*, 49801.

(12) Park, S.-J.; Kim, H.-S.; Jin, F.-L. Influence of fluorination on surface and dielectric characteristics of polyimide thin film. *J. Colloid Interface Sci.* **2005**, *282*, 238−240.

(13) Luo, L.; Hong, D.; Zhang, L.; Cheng, Z.; Liu, X. Surface modification of PBO fibers by direct fluorination and corresponding chemical reaction mechanism. *Compos. Sci. Technol.* **2018**, *165*, 106−114.

(14) Bei, R.; Qian, C.; Zhang, Y.; Chi, Z.; Xu, J.; Aldred, M. P. Highly transparent, strong, and flexible fluorographene/fluorinated polyimide nanocomposite films with low dielectric constant. *J. Mater. Chem. C* **2018**, *6*, 6378−6384.

(15) Toyokowa, F.; Shirataki, Y.; Ueda, M. A Novel Low Temperature Curable Photosensitive Polybenzoxazole. *Polym. J.* **2005**, *7*, 517−521.

(16) Lien-Chung Hsu, S.; Chen, W.-C. A novel positive photosensitive polybenzoxazole precursor for microelectronic applications. *Polymer* **2002**, *43*, 6743−6750.

(17) Fukukawa, K.; Ueda, M. Recent Development of Photosensitive Polybenzoxazoles. *Polym. J.* **2006**, *38*, 405−418.

(18) Reiser, A.; Huang, J. P.; He, X.; Yeh, T. F.; Jha, S.; Shih, H. Y.; Kim, M. S.; Han, Y. K.; Yan, K. The molecular mechanism of novolak-diazonaphtoquinone resists. *Eur. Polym. J.* **2002**, *38*, 619−629.

(19) Harman, G. *Wire Bonding in Microelectronics*; McGraw Hill Professional, 2009, 3.

(20) Wood, L.; Fairfield, C.; Wang, K., Plasma cleaning of chip scale packages for improvement of wire bond strength, *International Symposium on Electronic Materials and Packaging (EMAP2000)*; IEEE 2000, 406−408.

(21) Alberici, S.; Dellafiore, A.; Manzo, G.; Santospirito, G.; Villa, C. M.; Zanotti, L. Organic contamination study for adhesion enhancement between final passivation surface and packaging molding compound. *Microelectron. Eng.* **2004**, *76*, 227−234.

(22) Gulino, A.; Condorelli, G. G.; Mineo, P.; Fragala, I. An x-ray photoelectron spectra and atomic force microscopy characterization of silica substrates engineered with a covalently assembled siloxane monolayer. *Nanotechnology* **2005**, *16*, 2170−2175.

(23) Kaminker, R.; von Hatten, X. R.; Lahav, M.; Lupo, F.; Gulino, A.; Evmenenko, G.; Dutta, P.; Browne, C.; Nitschke, J. R.; van der Boom, M. E. Assembly of Surface-Confined Homochiral Helicates: Chiral Discrimination of DOPA and Unidirectional Charge Transfer. *J. Am. Chem. Soc.* **2013**, *135*, 17052−17059.

(24) Gulino, A.; Lupo, F.; Condorelli, G. G.; Amato, M. E.; Fragalà, M. E.; Scarlata, G. Reversible Photoswitching of Stimuli Responsive Si(100) Surfaces Engineered with an Assembled 1-Cyano-1-Phenyl-2-(4′-(10-Undecenyloxy)Phenyl)-Ethylene Monolayer. *J. Mater. Chem.* **2008**, *18*, 5011−5018.

(25) Gulino, A. Structural and Electronic Characterization of Self assembled Molecular Nanoarchitectures by X-ray Photoelectron Spectroscopy. *Anal. Bioanal. Chem.* **2013**, *405*, 1479−1495.

(26) Briggs, D.; Grant, J. T. *Surface Analysis by Auger and X-Ray Photoelectron Spectroscopy*; IMP: Chichester, UK, 2003.

(27) Greczynski, G.; Hultman, L. Compromising science by ignorant instrument calibration - need to revisit half a century of published XPS data. *Angew. Chem., Int. Ed.* **2020**, *59*, 5002−5006.

(28) Spitaleri, L.; Gangemi, C. M. A.; Purrello, R.; Nicotra, G.; Trusso Sfrazzetto, G.; Casella, G.; Casarin, M.; Gulino, A. Covalently conjugated gold−porphyrin nanostructures. *Nanomaterials* **2020**, *10*, 1644.

(29) Contino, A.; Maccarrone, G.; Spitaleri, L.; Torrisi, L.; Nicotra, G.; Gulino, A. One Pot Synthesis of Au_ZnO Core-Shell Nanoparticles Using a Zn Complex Acting as ZnO Precursor, Capping and Reducing Agent During the Formation of Au NPs. *Eur. J. Inorg. Chem.* **2018**, *43*, 4678−4683.

(30) Gengenbach, T. R.; Major, G. H.; Linford, M. R.; Easton, C. D. Practical guides for x-ray photoelectron spectroscopy (XPS): Interpreting the carbon 1s spectrum. *J. Vac. Sci. Technol., A* **2021**, *39*, No. 013204.

(31) Graf, N.; Yegen, E.; Gross, T.; Lippitz, A.; Weigel, W.; Krakert, S.; Terfort, A.; Unger, W. E. S. XPS and NEXAFS studies of aliphatic and aromatic amine species on functionalized surfaces. *Surf. Sci.* **2009**, *603*, 2849−2860.
(32) Tuccitto, N.; Riela, L.; Zammataro, A.; Spitaleri, L.; Li Destri, G.; Sfuncia, G.; Nicotra, G.; Pappalardo, A.; Capizzi, G.; Trusso Sfrazzetto, G. Functionalized Carbon Nanoparticle-Based Sensors for Chemical Warfare Agents. *ACS Appl. Nano Mater.* **2020**, *3*, 8182−8191.
(33) Nanséa, G.; Papirera, E.; Fiouxa, P.; Moguetb, F.; Tressaudb, A. Fluorination of carbon blacks: An X-ray photoelectron spectroscopy study: I. A literature review of XPS studies of fluorinated carbons. XPS investigation of some reference compounds. *Carbon* **1997**, *35*, 175−194.
(34) Zhang, T.; Hu, D.; Jin, J.; Yang, S.; Li, G.; Jiang, J. XPS study of PBO fiber surface modified by incorporation of hydroxyl polar groups in main chains. *Appl. Surf. Sci.* **2010**, *256*, 2073−2075.
(35) Wanga, H.; Liua, S.; Chunga, T.; Chenb, H.; Jeanb, Y.; Pramoda, K. P. The evolution of poly(hydroxyamide amic acid) to poly(benzoxazole) via stepwise thermal cyclization: Structural changes and gas transport properties. *Polymer* **2011**, *52*, 5127−5138.
(36) Giofrè, S. V.; Tiecco, M.; Celesti, C.; Patanè, S.; Triolo, C.; Gulino, A.; Spitaleri, L.; Scalese, S.; Scuderi, M.; Iannazzo, D. Eco-Friendly 1,3-Dipolar Cycloaddition Reactions on Graphene Quantum Dots in Natural Deep Eutectic Solvent. *Nanomaterials* **2020**, *10*, 2549.
(37) Dutta, A. Fourier transform infrared spectroscopy. *In Spectroscopic Methods for Nanomaterials Characterization*; Thomas, S., Thomas, R., Zachariah, A., Mishra, R., Eds.; Elsevier: Amsterdam, The Netherlands, 2017; 73−93.
(38) Gulino, A.; Papanikolaou, G.; Lanzafame, P.; Aaliti, A.; Primerano, P.; Spitaleri, L.; Triolo, C.; Dahrouch, Z.; Khaskhoussi, A.; Schiavo, S. L. Synthesis, characterization and photocatalytic behavior of SiO_2@nitrized-TiO_2 nanocomposites obtained by straightforward novel approach. *ChemistryOpen* **2021**, *10*, 1033−1040.
(39) Zhang, Y.; Mushtaq, N.; Fang, X.; Chen, G. In situ FTIR analysis for the determination of imidization degree of polyimide precursors. *Polymer* **2022**, *238*, No. 124416.
(40) Tanikella, R. V.; Sung, T.; Bistrup-Allen, S. A.; Kohl, P. A. Rapid Curing of Positive Tone Photosensitive Polybenzoxazole Based Dielectric Resin by Variable Frequency Microwave Processing. *IEEE Trans. Compon. Packaging Manuf. Technol.* **2006**, *29*, 411−419.
(41) Windrich, F.; Kappert, E. J.; Eichhorn, K. J.; Häubler, L.; Benes, N. E.; Voit, B. In-situ imidization analysis in microscale thin films of an ester-type photosensitive polyimide for microelectronic packaging applications. *Eur. Polym. J.* **2016**, *84*, 279−291.
(42) Kaminker, R.; Motiei, L.; Gulino, A.; Fragalà, I.; Shimon, L. J. W.; Evmenenko, G.; Dutta, P.; Iron, M. A.; van der Boom, M. E. Stepwise Assembly of Coordination-Based Metal−Organic Networks. *J. Am. Chem. Soc.* **2010**, *132*, 14554−14561.
(43) Choudhury, J.; Kaminker, R.; Motiei, L.; de Ruiter, G.; Morozov, M.; Lupo, F.; Gulino, A.; van der Boom, M. E. Linear vs Exponential Formation of Molecular-Based Assemblies. *J. Am. Chem. Soc.* **2010**, *132*, 9295−9297.
(44) Contino, A.; Maccarrone, G.; Fragalà, M. E.; Spitaleri, L.; Gulino, A. Conjugated Gold−Porphyrin Monolayers Assembled on Inorganic Surfaces. *Chem. − Eur. J.* **2017**, *23*, 14937−14943.
(45) Wolan, J. T.; Hoflund, G. B. Surface characterization study of AgF and AgF_2, powders using XPS and ISS. *Appl. Surf. Sci.* **1998**, *125*, 251−258.
(46) Lemoine, K.; Lhoste, J.; Hémon-Ribaud, A.; Heidary, N.; Maisonneuve, V.; Guiet, A.; Kornienko, N. Investigation of mixed-metal (oxy)fluorides as a new class of water oxidation electrocatalysts. *Chem. Sci.* **2019**, *10*, 9209.
(47) Zamora Zeledón, J. A.; Gunasooriya, G. T. K. K.; Kamat, G. A.; Kreider, M. E.; Ben-Naim, M.; Hubert, M. A.; Avilés Acosta, J. E.; Nørskov, J. K.; Stevens, M. B.; Jaramillo, T. F. Engineering metal−metal oxide surfaces for high-performance oxygen re-duction on Ag−Mn electrocatalysts. *Energy Environ. Sci.* **2022**, *15*, 1611.
(48) Fiorenza, R.; Spitaleri, L.; Gulino, A.; Scirè, S. High-Performing Au-Ag Bimetallic Catalysts Supported on Macro-Mesoporous CeO_2 for Preferential Oxidation of CO in H_2-Rich Gases. *Catalysts* **2020**, *10*, 49.
(49) Xue, D.; Wang, X.; Ni, H.; Zhang, W.; Xue, G. Surface Segregation of Fluorinated Moieties on Random Copolymer Films Controlled by Random-Coil Conformation of Polymer Chains in Solution. *Langmuir* **2009**, *25*, 2248−2257.
(50) Liu, D.; Chen, P.; Chen, M.; Yu, Q.; Lu, C. Effects of argon plasma treatment on the interfacial adhesion of PBO fiber/bismaleimide composite and aging behaviors. *Appl. Surf. Sci.* **2011**, *257*, 10239−10245.

https://doi.org/10.1021/acsomega.3c00952
ACS Omega 2023, 8, 15586−15593